Robustness of the enhanced magnetic anisotropy in Ni nanowires regardless of the deposition potential

Y. Velázquez-Galván

División de Materiales Avanzados, Instituto Potosino de Investigación Científica y Tecnológica A. C., Camino a la Presa 2055, 78216 San Luis Potosí, SLP, México

J. de la Torre Medina

Instituto de Investigaciones en Materiales / Unidad Morelia, Universidad Nacional Autónoma de México. Antigua Carretera a Pátzcuaro No. 8701 Col. Ex Hacienda de San José de la Huerta, 58190 Morelia, Mexico

L. Piraux

Institute of Condensed Matter and Nanosciences, Université catholique de Louvain, Place Croix du Sud 1, B-1348, Louvain-la-Neuve, Belgium

A. Encinas

División de Materiales Avanzados, Instituto Potosino de Investigación Científica y Tecnológica A. C., Caminio a la Presa 2055, 78216 San Luis Potosí, SLP, México

Abstract

The effects of the deposition potential on the structural and magnetic properties of Ni nanowires with a diameter of 40 nm and lengths varying from 16 up to 56 μm have been studied. The results show that very long NWs exhibit a large enhancement of their uniaxial magnetic anisotropy. This anisotropy reaches values as high as 1.6×10^6 erg/cm^3 that is comparable with the value due to the magnetostatic anisotropy contribution ($\approx 5\times10^6$ erg/cm^3) and as shown from the results this large anisotropy is practically insensitive to the deposition potential. Moreover, as shown on shorter NWs, this enhancement of the anisotropy is not observed and interestingly the potential does induce

*Corresponding author

Email address: yenni.velazquez.g@gmail.com (Y. Velázquez-Galván)

structural changes that relate to their magnetic properties. The enhanced anisotropy observed in long NWs is a robust effect as it is independent of the potential, making this property attractive for applications where high uniaxial anisotropies are required.

Keywords: Nanowires, Nickel, enhanced anisotropy, confinement, deposition potential

1. Introduction

Electrodeposited magnetic NWs are of great scientific and technological interest due to their simple cylindrical geometry and relative ease of fabrication. Electrochemical deposition into nanoporous templates has proven to be a very versatile approach to fabricate a wide variety of nanostructures based on cylindrical wires with novel physicochemical properties [1, 2, 3, 4, 5, 6, 7].

Nickel NWs are amongst the most interesting and promising magnetic NWs, due to their environmentally benign nature, low cost and availability. At present there are numerous reports on their physicochemical properties that show their potential. Furthermore, oxidised Ni NWs have been shown to posses great potential for memristive elements as well as for their use as electrochemical electrodes for energy (batteries [8] and supercapacitors [9, 10]) and sensing (glucose [11, 12, 13] and urea [14, 15, 16]).

The magnetic and electronic properties of Ni NWs are strongly dependent on their crystalline structure, which in turn are related to their use in different applications. Numerous studies have shown that it is possible to control the magnetic properties of these systems changing a variety of parameters as the host matrix [17, 18, 19, 20], diameter [21, 22, 23, 24, 25], length or aspect ratio [26, 27] as well as the pH [28, 29, 30], temperature [31] and applied potential [32, 33, 34, 35].

Recently it was shown that very long Ni nanowires (with lengths of about 10-80 μm) grown in anodic aluminium oxide (AAO) templates exhibit a very large enhanced uniaxial magnetic anisotropy [36]. This anisotropy was shown to originate from the combination of two effects. The first one is related to a two stage growth mechanism in which the NWs first grow with a polycrystalline microstructure which after reaching a certain length evolves to a single-crystalline [110] structure [17, 37, 38]. The second effect was related to a residual stress on NWs that results from their confined growth which increases as the diameter decreases and as the crystal texture is enhanced

[39, 40]. This enhanced anisotropy was reported to be as high as 1.4×10^6 erg/cm^3 (or 5.7 kOe) which is comparable to the effective magnetic anisotropy of Co. Such large anisotropy opens up many interesting perspectives where nanomaterials with high uniaxial anisotropies are desirable. This is further complemented by other valuable properties of Ni, like its availability, low cost compared with Co and greater stability as compared to Fe. Furthermore, this enhanced anisotropy was shown to depend on geometrical parameters such as NW diameter and length which relate to the microstructure [22, 41, 42]. In this sense, as shown by several studies, the microstructural characteristics of electrodeposited Ni NWs depends strongly on the deposition potential [38, 32, 33]. However, most (if not all) of the studies regarding the influence of the deposition potential on the structural and magnetic properties have been limited of short Ni NWs, in the range 6–12 μm [30, 43, 44, 45, 46]. So in this sense, analyzing the effect of the deposition potential on very long Ni NWs on the microstructural and magnetic properties is relevant since there is no information regarding its effect on the value of the enhanced uniaxial magnetic anisotropy. In addition also seeking to determine if similar effects can be obtained in other templates, particularly in polycarbonate (PC) membranes which are also interesting due to their lower pore densities and their flexibility.

In the present work we have studied the influence of the deposition potential on the structural and magnetic properties of arrays of Ni NWs electrodeposited in porous AAO and PC membranes. We have shown that neither the crystal orientation nor the large magnetic anisotropy of Ni NWs embedded in AAO membranes are significantly perturbed by the reduction potential. This magnetic anisotropy reaches a value as large as 1.6×10^6 erg/cm^3 (6 kOe), which is consistent with previous results [36]. Conversely, Ni NWs embedded in PC membranes do not show an enhanced anisotropy. These NWs have lower length ($\sim 15\mu$m) and they show significant changes in their structural and magnetic properties induced by the electrodeposition potential. These different behaviors are attributed to the two stage electrodeposition growth mechanism, which is related to the type of host template used for the growth of the NWs, as they limit the NW lengths. Therefore, the fundamental outcome of this work is the possibility of fabricate arrays of Ni NWs with a large uniaxial magnetic anisotropy independently of the deposition potential, allowing their fabrication using less restrictive deposition conditions.

2. Materials and methods

Ni NWs have been grown by electrodeposition into low pore density polycarbonate membranes (it4ip S. A.) as well as in high pore density anodic aluminum oxide membranes (Synkera Technologies, Inc.). PC based Ni NWs have a diameter of 40 nm, thickness of 20 μm and membrane porosity (NW packing fraction) P=5 % corresponding to an average interwire distance of d_0=165 nm, while NWs grown in AAO membranes have a diameter of 35 nm, thickness of 90 μm, P=12% and d_0=95 nm. All depositions were done at room temperature in the potentiostatic mode using a Ag/AgCl reference electrode and a Pt counter electrode. For the electrodeposition process, a Cr(5nm)/Cu(600nm)/Au(300nm) layer was evaporated on one side of the membrane in order to serve as a cathode. The electrolyte contained 262.84 g/l $NiSO_4 \cdot 6H_2O$ + 30 g/l H_3BO_3 with a pH value of 4.0. For both PC and AAO based nanowire samples, the electrodeposition was carried out at constant deposition potentials of -1.0, -1.05, -1.1, -1.2, -1.3, -1.4 and -1.5 V.

Characterization of the crystal structure was made by X-Ray Diffraction (XRD) with a CuKα radiation ($\lambda = 1.54\mathring{A}$) using a Rigaku smartkab X-ray diffractometer. The magnetic properties of the Ni NWs have been measured at room temperature using magnetometry and ferromagnetic resonance (FMR). The hysteresis loops were obtained by applying a magnetic field parallel to the wire axis, using an Alternating Gradient Magnetometer with a maximum applied field of $\pm$ 14 kOe. Field-swept FMR was done using a micro-strip line configuration with the external field applied parallel to the wire axis [47]. The absorption spectra are recorded at a constant excitation frequency while the applied field is swept from 10 kOe down to zero field. For a given excitation frequency, the resonance field corresponds to the minimum of the spectra. Then, to construct the dispersion relation, the absorption spectra are measured and recorded using different excitation frequencies.

3. Results

3.1. Effect of the potential in AAO based-Ni NWs

Figures 1 (a) and (b) show SEM micrographs of the cross-sectional view of electrodeposited Ni NWs embedded in AAO membrane. As seen in the figure, the nanowires grow perpendicular to the Au layer inside the pores of

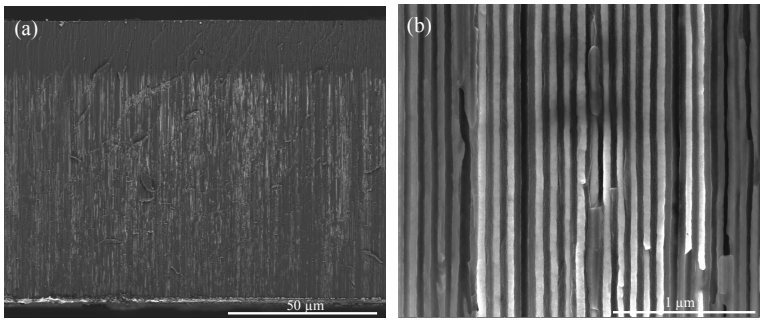

Figure 1: (a) Low and (b) high magnification SEM micrographs of the cross-section of electrodeposited Ni NWs embedded in AAO membrane.

the membrane. Further, it is possible to observe the length of the nanowires and the membrane thickness.

Figure 2 shows the XRD measurements obtained in Ni NW arrays grown using AAO templates at different deposition potentials ranging from -1.0 to -1.5 V. As seen in the figure, Ni NWs grown in AAO templates show little sensitivity to the deposition potential, in all cases a strong [110] texture due to the presence of the peak to the (220) plane is observed. Furthermore, the (200) reflection is also noticeable but its amplitude is very small in all cases. On the other hand, the contribution due to the Au layer deposited in one side of the membrane is perceptible and its intensity depends on how much it can be removed from this layer before characterizing the samples. From the results it follows that the texture quality is best at E=-1.0 to -1.05 V.

Texture analysis was done in order to quantify this strong preferential crystallographic orientation. The texture coefficients were determined using the XRD patterns and Harris formula defined as [48]

$$TC(hkl)_i = \frac{\frac{I(hkl)_i}{I_0(hkl)_i}}{\frac{1}{N}\sum_n \frac{I(hkl)_n}{I_0(hkl)_n}}, \tag{1}$$

where *TC(hkl)* is the texture coefficient of (*hkl*) plane, $I(hkl)_i$ is the measured relative intensity, $I_0(hkl)$ is the relative intensity of the corresponding plane for a pollycrystalline sample and N is the total number of reflections. In this work, the Ni NWs were indexed using the 00-004-0850 card (ICDD PDF-4 database)[49]. The texture coefficient with values larger than the unity indicates a preferred orientation of the nanowire arrays along the corresponding

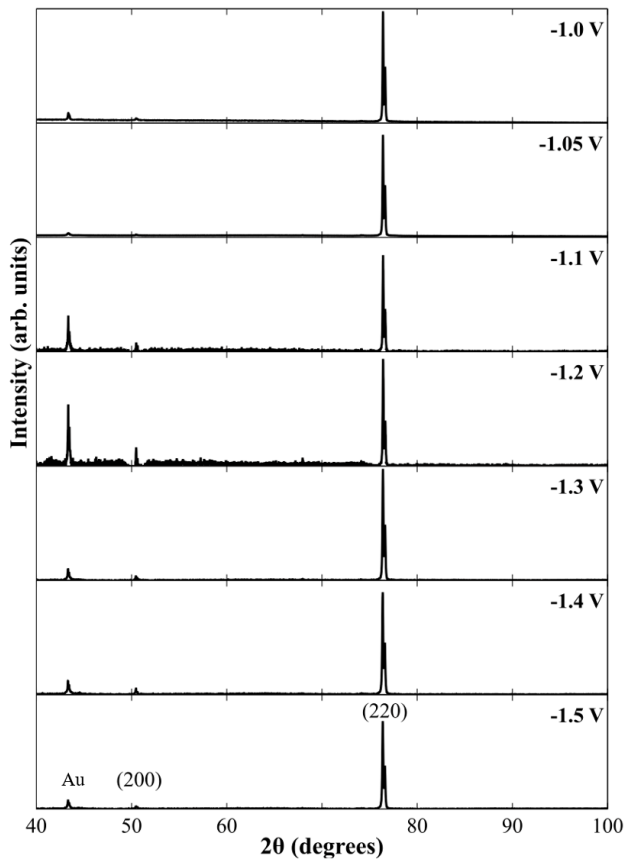

Figure 2: XRD patterns from Ni NWs embedded in AAO membranes grown at deposition potentials of E = -1.0, -1.05, -1.1, -1.2, -1.3, -1.4 and -1.5 V.

plane. Further, the maximum value of *TC(hkl)* is N which implies that the wires posses a complete preferential orientation [50].

The results obtained using XRD patterns of figure 2 give TC(200) values ranging from 0.04 to 0.16 and TC(220) values around 1.9 for Ni NWs grown in AAO membranes. These texture coefficient values are consistent with a strong texture with preferential crystallographic orientation along the [110] direction regardless of the deposition potential.

Figure 3 (a) shows the hysteresis loops measured with the external field applied parallel to the axis of the NWs embedded in AAO templates at deposition potentials of E=-1.0, -1.2 and -1.5 V. Furthermore, figures 3 (b-

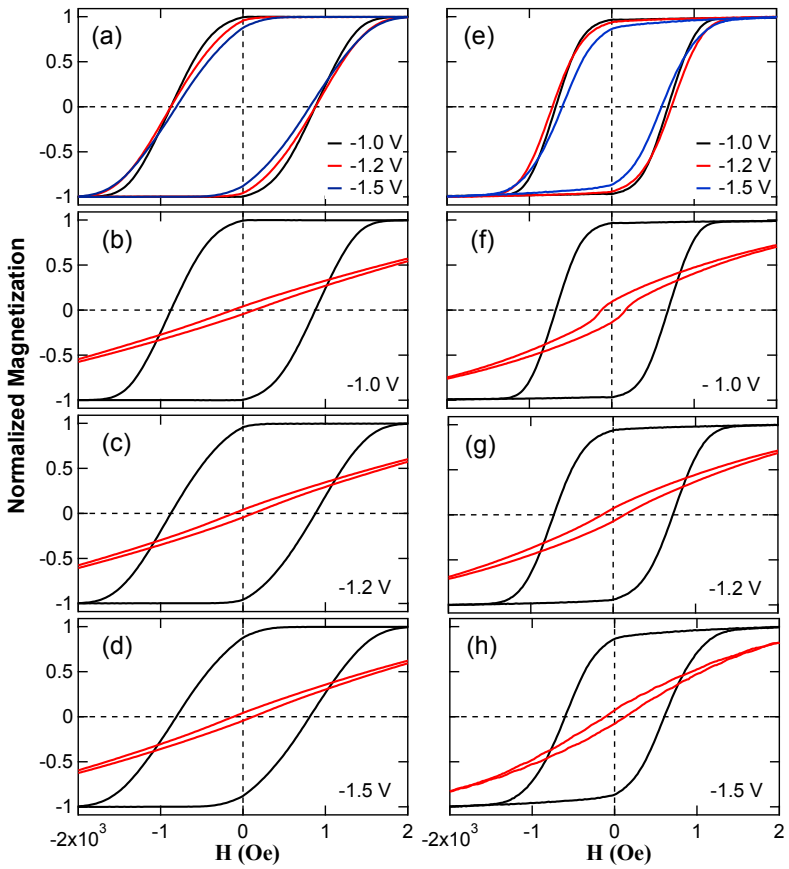

Figure 3: Hysteresis loops measured with the field applied parallel to the NW axis for Ni wires grown at deposition potentials of E = -1.0, -1.2 and -1.5 V vs Ag/AgCl in (a) AAO and (e) PC templates. Comparison of the hysteresis loops measured with the magnetic field applied parallel and perpendicular to the NW axis for the Ni NWs deposited in (b-d) AAO and (f-h) PC templates.

d) show the hysteresis loops obtained by applying the magnetic field parallel and perpendicular to the NWs axis for the samples deposited at potentials E= -1.0, -1.2 and -1.5 V in AAO templates. The remanence (M_r/M_s) as well as the coercive field (H_c) show slight changes when the potential becomes more negative, suggesting a decrease in the total anisotropy.

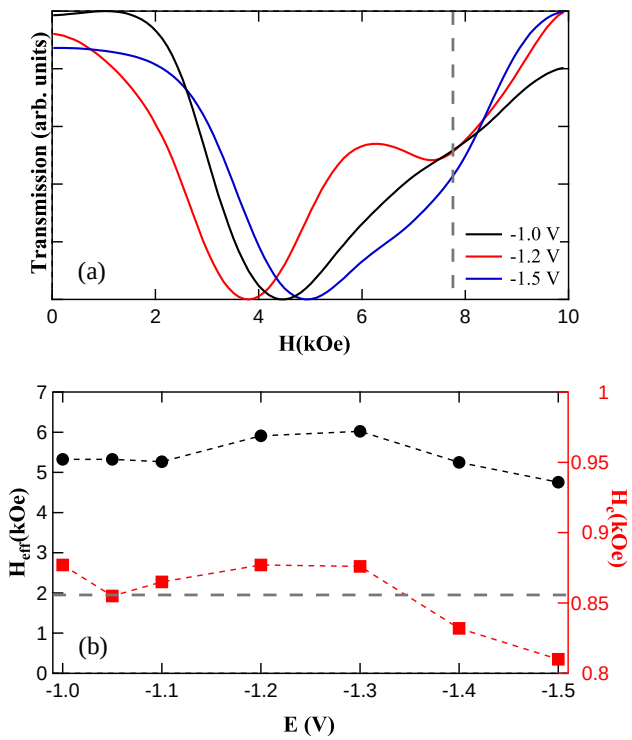

Figure 4: (a) Ferromagnetic resonance spectra recorded at 30 GHz in Ni-AAO NWs (d=35 nm and P=12%) obtained using deposition potentials of E=-1.0, -1.2 and -1.5 V, the vertical dashed line corresponds to the resonance field given by equation (2) and, (b) comparison between the effective anisotropy field and the coercive field with variation of electrodeposition potential, the horizontal dashed line indicates the MS anisotropy contribution.

Figure 4 (a) shows typical FMR spectra recorded at 30 GHz for the same samples as in Fig. 3. As seen in the figure, the lineshape of the FMR spectra changes significantly as a function of the deposition potential. In all cases, the linewidth is large and two absorption peaks can be identified, which is more evident in the E=-1.2 V sample. The presence of two absorption peaks

in the FMR spectra indicates the presence of two Ni volume fractions each with different magnetic anisotropy. Moreover, the amplitude of these peaks are proportional to the individual volume fractions [36]. As seen in the figure, all the spectra show a dominant absorption peak located at lower field values, while the second low-intensity peak appears at higher fields.

In order to relate the position of these peaks with their corresponding magnetic anisotropies, consider the FMR dispersion relation for cylindrical NWs with the field applied parallel to the wires,

$$\frac{f}{\gamma} = H_r + H_{eff}, \tag{2}$$

where f is the excitation frequency, γ=3.09 GHz/kOe is the gyromagnetic ratio for Ni [51] and H_{eff} is the effective field. The effective field includes all the magnetic anisotropy contributions as well as the dipolar interaction between NWs. For magnetic NWs, the magnetic anisotropy can have shape, magnetocrystalline (MC) and magnetoelastic (ME) contributions. For the particular case of very long Ni NWs where there are no MC or ME contributions, the effective field is purely magnetostatic (MS) since it contains only the shape anisotropy ($H = 2\pi M_s$) and the dipolar interaction ($H = -6\pi M_s P$), namely [47],

$$H_{ms} = 2\pi M_s(1 - 3P), \tag{3}$$

where M_s=485 emu·cm^{-3} is the saturation magnetization of Nickel [52]. The MS field serves as a reference to analyze the position of the FMR peaks. For the Ni NWs grown in AAO, the packing fraction is P=12% so their resonance field at 30 GHz is H_r=7.76 kOe, which corresponds to the vertical dashed line in Fig. 4(a). From the figure it is clear that the high-field low amplitude FMR peaks are located around the expected value for purely MS Ni nanowires. The major absorption peaks, with lower resonance fields imply an additional anisotropy contribution that leads to a larger effective field. The field difference between the resonance fields of these peaks and the position of the MS resonance provide an estimate of the magnitude of this additional anisotropy contribution, which in this case is in the order of 3-4 kOe. This enhanced anisotropy in Ni NWs grown in AAO templates originates from a residual stress due to the confinement in small pore diameter templates [36]. This large anisotropy was observed in all the Ni AAO samples. Figure 4 (b) shows the effective field obtained using Eq. (2) and the coercive field of the Ni AAO samples as a function of the deposition potential. The

dashed horizontal line is the MS effective field for a Ni NWs array with a packing fraction of 12%. The effective field increases up to a maximum value as the potential increases from -1.0 V up to -1.2 V, which is followed by a decrease of about 1.3 kOe as the potential further increases. Furthermore, it is observed that both H_c and H_{eff} show a similar behavior due to the deposition potential. This shows that the enhanced anisotropy in AAO Ni NWs is little sensitive to the deposition potential. Indeed, for all deposition potentials a very large anisotropy is observed which varies little. Comparing the measured effective field values with that expected for the MS case, an enhancement of 3-4 kOe is confirmed. Considering the same packing fraction, this value is comparable to the MS field of cobalt obtained using Eq. (3) and M_s=1400 emu·cm^{-3}, which is around 5.6 kOe.

3.2. Effect of the potential in PC-based Ni NWs

Figure 5 shows the XRD measurements corresponding to Ni NW arrays grown using PC templates at different deposition potentials. As observed, the crystalline structure of these NWs is polycrystalline as suggested by the presence of (220) and (111) planes in the diffractograms. Nickel nanowires grown at low reduction potentials in PC membranes are highly polycrystalline, with a crossover at -1.3 V where they become mostly single-crystalline with preferential crystal orientation along the [110] direction. Further increasing the deposition potential, at -1.4 V and -1.5 V, there is a shift on the preferential orientation from [110] to [111] direction because the peak corresponding to the (111) plane becomes more pronounced and the (220) plane is almost negligible. No changes are observed in the weak (200) plane due to the applied potential. These diffraction peaks are in agreement with 00-004-0850 card (ICDD PDF-4 database) [49].

These features have been corroborated with a quantitative analysis of the texture coefficients determined using Eq. (1) with N=4 for all the XRD patterns of figure 5.The results are summarized in Table 1 for (111) and (220) planes. In this case, the texture coefficient values are greater than one for TC(111) and TC(220). The texture coefficient values of the other reflections are less than one for all the arrays and therefore are not shown in Table 1. It shows that Ni NWs arrays deposited in PC membranes can be obtained with a texture having either a (111) or a (220) preferential orientation. Ni NWs embedded in PC membranes grown at low deposition potentials present a texture that appears to be approximately constant along the (220) plane. The maximum texture value is obtained for the arrays deposited at -1.3 V

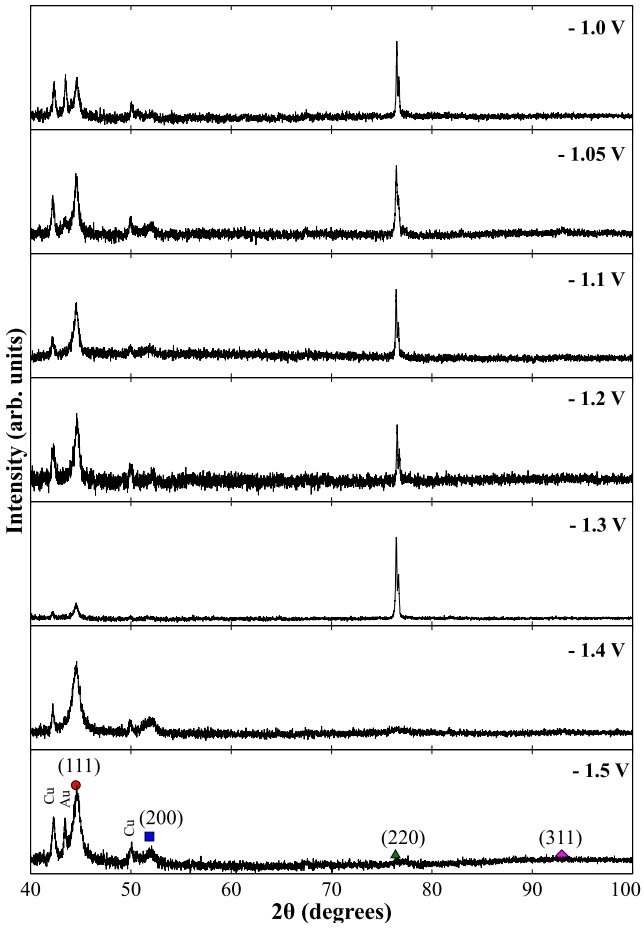

Figure 5: XRD patterns from Ni NWs embedded in PC membranes grown at deposition potentials of E = -1.0, -1.05, -1.1, -1.2, -1.3, -1.4 and -1.5 V. The dots positioned on the graph for the -1.5V sample correspond and are in agreement with the expected position and intensity of the (111), (200) and (220) peaks for polycrystalline Ni [49].

which indicates a strong texture with preferential crystal orientation along the [110] direction. On the other hand, NWs deposited at higher potentials exhibit a texture along the [111] direction as expected.

Table 1: Texture coefficient values for Ni NWs embedded in PC membranes grown at different deposition potentials.

E(V)	TC(111)	TC(220)
-1.0	0.30	2.88
-1.05	0.47	2.55
-1.1	0.44	2.52
-1.2	0.55	2.29
-1.3	0.17	3.33
-1.4	1.11	1.20
-1.5	1.23	0.98

Figure 3 (e) shows the hysteresis loops of Ni NWs grown in PC templates at deposition potentials of E=-1.0, -1.2 and -1.5 V with the external field applied along the NWs axis. As seen in the figure, small changes in both the remanence and coercive field appear as the deposition potential is modified, which is similar to the behavior observed in the AAO based samples. As a comparison, the hysteresis loops with the field applied parallel and perpendicular to the NWs grown using a deposition potential of E=-1.0, -1.2 and -1.5 V grown in PC membranes are shown in figures 3 (f-h).

Complementary information about the magnetic anisotropy of these systems is obtained from FMR spectra recorded at 26 GHz. As seen in Fig. 6 (a), the absorption spectra display a complex non-symmetric lineshape, a small peak besides the main absorption peak is observed. This feature is more pronounced at lower potentials and indicates that Ni NWs present two different magnetic anisotropy contributions. Contrary to the case of the AAO based arrays of Ni NWs, all the PC based samples display a dominant absorption peak at higher resonance fields. This opposite behavior arises from lower length of the NWs, then corroborating their polycrystallinity which is in good agreement with previous results [36]. The lineshape and position of the minimum of the FMR spectra shown in Fig. 6 (a) are consistent with a magnetic behavior characteristic of polycrystalline NWs that is mainly dominated by the MS contribution.

To further investigate the magnetic behavior of the PC based Ni NWs,

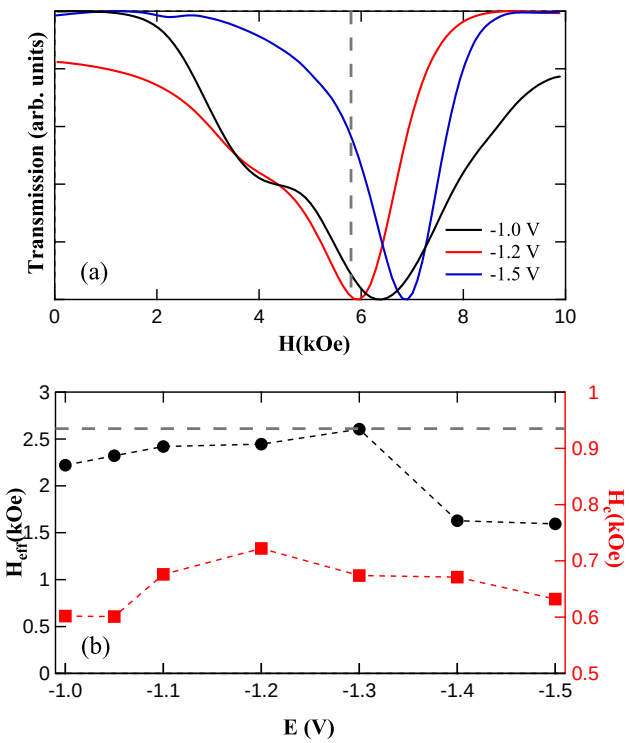

Figure 6: (a) Room temperature absorption spectra recorded at 26 GHz for Ni NWs grown in PC membranes (d=40 nm and P=5%) obtained using deposition potentials of E= -1.0, -1.2 and -1.5 V, the vertical dashed line correspond at the resonance field with only MS anisotropy contribution and, (b) comparison between the effective anisotropy field and the coercive field as a function of the applied potential, the horizontal dashed line indicates the effective anisotropy field for systems with only MS anisotropy contributions.

Fig. 6 (b) shows the effective anisotropy field, H_{eff}, as a function of the deposition potential determined using Eq. (2). For this system, the effective field increases with the deposition potential toward the observed limiting value for arrays of Ni NWs with purely MS anisotropy, at a potential of -1.3 V. Then, this field decreases at values still lower than those for arrays deposited at low potentials. Particularly, the effective field for the NWs deposited at higher potentials is about 1 kOe lower than the expected value due only to the MS anisotropy contribution (see the horizontal dashed line). This decrease in magnetic anisotropy indicates the presence of an additional anisotropy contribution that competes with the intrinsic MS anisotropy of the NWs. That is, the shift in the anisotropy is related with the changes observed in the crystalline structure, as seen in Fig. 5, where the (220) texture disappears for Ni NWs deposited at higher potentials.

Furthermore, the variation of the coercive field with the reduction potential is displayed in Fig. 6 (b) for comparison. As seen, this field shows the same trend as that for H_{eff}, where a maximum value is also observed around -1.3 V. It can be also observed that although the coercive field presents small variations due to the potential, its behavior is similar to the observed in the effective field as expected. Moreover, H_c values of these NWs arrays embedded in PC are slightly lower than the ones for NWs grown in AAO.

4. Discussion

The results presented show that Ni NWs embedded in AAO membranes exhibit a large enhancement of the magnetic anisotropy [36]. This anisotropy corresponds to values of the same order of magnitude and comparable to the MS anisotropy for arrays of Co NWs ($\approx$ 5600 Oe)[51, 23]. In contrast, for arrays of short Ni NWs grown in PC membranes no such a large enhancement of the magnetic anisotropy is observed.

As shown previously, the large positive enhancement of the magnetic anisotropy of Ni NWs is strongly related with a two stage electrodeposition growth of the Ni NWs [36, 53, 38, 33]. In the initial growth stage, the orientation of the individual 3D nuclei is random, which is then followed by an alignment of crystal planes along a preferential direction in a 2D growth mode, leading to a structural transition of the nanowires from polycrystalline to single-crystalline [54]. Therefore the texture of thicker metal deposit is the result of a competitive growth mechanism occurring in the subsequent growth stage to the coalescence stage.

The length of the polycrystalline segment can be obtained as a function of the total length of the NWs using the previously reported expression, given by

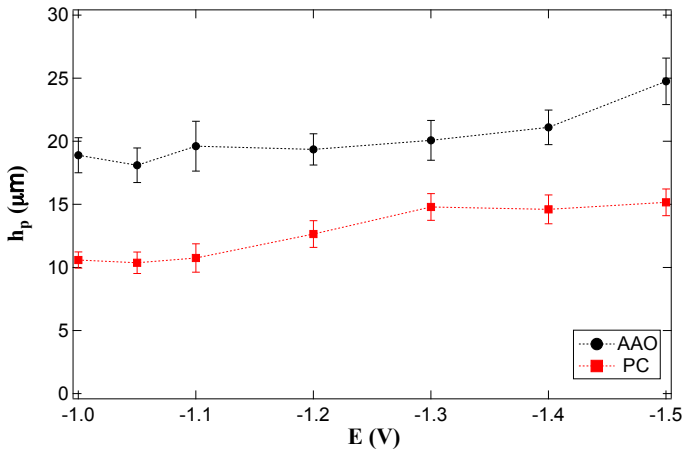

Figure 7: Length of the polycrystalline segment (h_p) as a function of the electrodeposition potential for Ni NWs grown in AAO and PC templates.

$$h_p = \frac{h}{1+r}, \tag{4}$$

where $r{=}h_s/h_p$ is the ratio between the length of the single and polycrystalline segments [36]. The total length of the NWs, h, growth in AAO and PC membranes is 55 μm and 15 μm, respectively. Figure 7 shows the variation of h_p as a fuction of the electrodeposition potential for Ni NWs growth in AAO and PC membranes. As observed, the length of the polycrystalline segment increases with the potential for both systems. This behavior is in agreement with the decrease of the effective anisotropy field as the negative potential is increased, as seen in Fig. 4(b) and 6(b). Furthermore, in the case of NWs embedded in PC membranes h_p tends to a maximum value of about 15 μm at more negative potentials, which corresponds to almost the total length of the NWs ($h_p \approx h$).

The structural changes observed in the arrays of Ni NWs are further evidenced on their magnetic properties. Single-crystalline Ni NWs grown in AAO membranes display higher coercive field and remanence magnetization values than for polycrystalline Ni NWs grown in PC membranes, which is

consistent with previous works [33]. In general, the coercive field of Ni NWs in AAO membranes is larger than that of Ni NWs in PC membranes because the magnetic anisotropy of the former is much larger than that of the later. This difference in magnetic anisotropy is explained by the difference of the effective ME contributions in each system. The high aspect ratio of the NWs in AAO membranes confers a large positive ME effect that lies along the NWs axis and adds to the intrinsic MS contribution [36]. Conversely, the ME contribution of lower aspect ratio NWs in PC membranes is negligible and not necessarily lies along the NWs axis, so it competes with the MS contribution leading to a lower effective magnetic anisotropy.

To further investigate the additional magnetoelastic energy observed in both systems, the magnetoelastic field can be obtained directly from H_{eff} in Fig. 4 (b) and 6 (b), using the expression

$$H_{me} = H_{eff} - H_{ms}, \tag{5}$$

where H_{ms} is given in Eq. (3). However, the comparison of the additional ME anisotropy contribution with previous results is easier in terms of the ME energy [36], $K_{me} = (H_{me} \times \mathrm{M}_s)/2$. Figure 8 shows K_{me} as a function of the deposition potential (E) of Ni NWs embedded in PC and AAO templates, determined using Eq. (2). The behavior of K_{me} with E is similar for both systems, because the ME energy increases with E up to a maximum value at -1.3 V and then decreases at more negative values. The observed variation in K_{me} with E is of about 2.5×10^5 erg·cm^{-3}. The very similar lineshape of K_{me} vs E for arrays of NWs in both PC and AAO membranes, suggests that such variation is due to the polycrystalline segment of the NWs. That is, in Ni NWs embedded in PC membranes there is not a subsequent single-crystalline segment that could explain such a variation. Therefore, the deposition potential is responsible of structural changes in the polycrystalline segment, which are related with the observed changes of K_{me}. Besides, for the case of long Ni NWs in AAO membranes, its effective ME energy is the superposition of two main ME contributions that arise from both crystalline segments. The single-crystalline segment leads to a large positive ME contribution, whereas the polycrystalline segment leads to a low ME contribution. Specifically, for the polycrystalline segment the ME contribution arises from the superposition of contributions of different crystal planes under residual stress. Then, changing the deposition potential gives rise to microstructural changes and variations of the ME anisotropy of this segment. For instance,

no polycrystalline ME contribution is induced for E= -1.3 V, as seen in Fig. (8) for the case of Ni NWs in PC membranes.

Furthermore, since the observed changes in K_{me} vs E for Ni NWs in AAO membranes (see Fig. 8) arise only from variations of the ME contribution of the polycrystalline segment, the strong positive ME contribution of the single-crystalline segment is invariant to changes in the deposition potential. Therefore, the large magnetic anisotropy enhancement in AAO based composites can be always achieved regardless of the electrodeposition conditions, with the only condition that long enough NWs have to be grown in order to promote the nucleation of the single-crystalline segment.

Besides, for both AAO and PC based NW arrays the decrease of K_{me} at $|E| > 1.3$ V, is related with the structure evolution from compact towards more porous structure due to the enhanced electrochemical hydrogen evolution [55, 32, 37]. The same feature is found for PC and AAO-based NW arrays which leads to a similar reduction of the magnetostatic coupling and corresponding magnetic anisotropy, as shown in Fig.8. However, for AAO-based NW arrays, the estimated value of K_{me} remains positive following the dominant contribution of the ME effect associated to the presence of single-crystalline segment. Moreover, from the lowest to the highest potential we observe that their magnetic anisotropy contribution increases, reaches a maximum value and then decreases. This variation is consistent with the behavior of the coercivity and remanence in the major hysteresis loop.

In general, the main phases observed in Ni NWs are (111), (220) and (200). As expected, NWs grown in AAO membranes are consistent with the presence of the (220) plane. While PC based NWs are mostly polycrystalline, they also show a correlation between the increase of the amount of (111) grains and the decrease in their anisotropy.

The structural changes in the Ni NWs due to the deposition potential can be explained by a complex interplay between a hydrogen adsorption, the surface energy and work function of various crystal planes [38, 56]. During the electrochemical process, there are different reactions of the competitive discharge between Ni^{2+} and H^{+} ions [57, 55]. This growth competition and the variation of the applied potential leads to a change in the composition of the NWs that is associated with the predominance inside of the cathodic layer of chemical species which results from the hydrogen co-deposition. As observed, long NWs (AAO) are single-crystalline with a preferential growth along the [110] direction, which is more favorable due to the fact that both its work function and the H^{+} ions absorption are low for this plane [58].

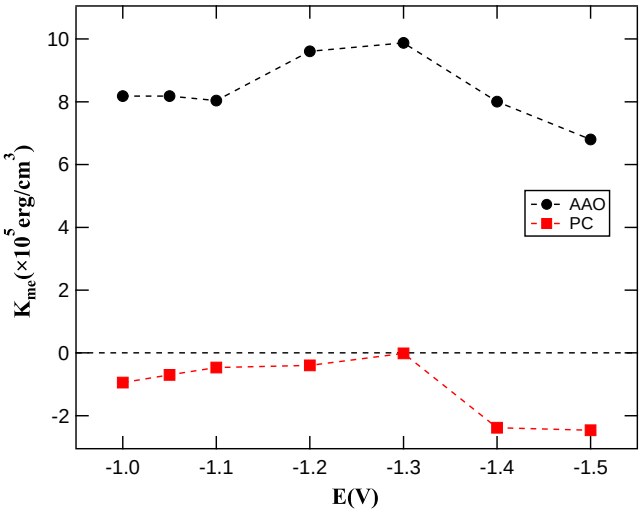

Figure 8: Variation of the magnetoelastic anisotropy energy K_{me} with the applied potential for Ni NWs grown in AAO and PC templates.

Moreover, the intensity of this plane is predominant regardless the applied potential. Conversely, short NWs (PC) grown at high potentials present a polycrystalline structure, which is in agreement with the Ni-fcc polycrystalline face [59]. Changes in the NWs crystal structure are related with the variation of the deposition potential, which influences the growth nucleation rate of Ni ions. Then, the growth of the polycrystalline segment with the more pronounced peak corresponding to the (111) plane, is favoured at ions larger deposition rates due to the abscense of active sites or blocking of metal by hydrogen bubbles during the electrodeposition process, which fairly explains the behavior of Ni NWs grown at deposition potentials $|E| > 1.3$ V [32, 38].

5. Conclusion

The effect of the deposition potential on the structural and magnetic properties of Ni NWs have been studied with particular interest in the enhanced uniaxial magnetic anisotropy obtained in very long NWs. To this end Ni NWs grown in AAO and PC nanoporous templates were considered. For the longest Ni NWs grown in AAO, two distinct structural phases are obtained. First a polycrystalline phase grows during the first stage of deposition, which

after attaining a certain critical length changes to a single-crystalline structure with a preferential orientiation in the [110] direction. This two-stage growth mechanism leads to the enhanced magnetic anisotropy. The results show that once the microstructure changes from poly to single crystal the enhancement of the magnetic anisotropy is practically insensitive to the deposition potential. On the contrary, as seen for the shorter NWs grown in PC templates, when the critical length where the structure changes from poly to single crystal is not reached, there is no enhancement of the magnetic anisotropy. Moreover, the polycrystalline segment of the Ni deposits is affected by the deposition potential. Our results show that the large uniaxial magnetic anisotropy in arrays of Ni NWs have an inherent relation with their size and confinement, this provide an interesting tool to develop nanoscale materials with high magnetic anisotropy.

Acknowledgements

The authors thank R. Legras and E. Ferain of it4ip S. A. for providing the PC membranes as well as LINAN-IPICYT for access to their facilities and Beatriz Rivera Escoto for her technical assistance with the XRD. Y. Velázquez-Galván thanks Fondo CONACYT- Secretaría de Energía - Hidrocarburos. This work was partly supported by CONACYT projects CB-177896 and CB-286626, the UNAM-PAPIIT IN106619, the Fédération Wallonie-Bruxelles (ARC 13/18-052, Supracryst) and the National Fund for Scientific Research (FNRS).

[1] A. Huczko, *Appl. Phys. A*, 2000, **70**, 365.

[2] K. Nielsch, F. Müller, A.-P. Li and U. Gösele, *Adv. Mater.*, 2000, **12**, 582.

[3] C.-G. Wu, H. L. Li and N.-L. Shau, *J. Solid. State Electrochem.*, 2006, **10**, 198.

[4] M. E. Toimil-Morales, *Beilstein J. Nanotechnol.*, 2012, **3**, 860–863.

[5] M. I. Irshad, F. Ahmad, N. M. Mohamed and M. Z. Abdullah, *Int. J. Electrochem. Sci.*, 2014, **9**, 2548–2555.

[6] C. R. Martin, *Chem. Mater.*, 1996, **8**, 1739–1746.

[7] M. Kac, A. Zarzycki, S. Kac, M. Kopec, M. Perzanowski, E. M. Dutkiewicz, K. Suchaneka, A. Maximenko and M. Marszalek, *Mater. Sci. Eng., B*, 2016, **211**, 75–84.

[8] A. Vlad, V.-A. Antohe, J. M. Martinez-Huerta, E. Ferain, J.-F. Gohy and L. Piraux, *J. Mater. Chem. A*, 2016, **4**, 1603.

[9] D. Su, H.-S. Kim, W.-S. Kim and G. Wang, *Chem. Eur. J.*, 2012, **18**, 8224–8229.

[10] S. Xu, C. Su, T. Wang, Y. Ma, J. Hu, J. Hu, N. Hu, Y. Su, Y. Zhang and Z. Yang, *Electrochim. Acta*, 2018, **259**, 617–625.

[11] X. Niu, M. Lan, H. Zhao and C. Chen, *Anal. Chem.*, 2013, **85**, 3561–3569.

[12] K. E. Toghill and R. G. Compton, *Int. J. Electrochem. Sci.*, 2010, **5**, 1246–1301.

[13] X. Wang, Y. Zhang, C. E. Banks, Q. Chen and X. Ji, *Colloids Surf., B*, 2010, **78**, 363–366.

[14] F. Guo, K. Ye, K. Cheng, G. Wang and D. Cao, *J. Power Sources*, 2015, **278**, 562–568.

[15] J. Hubalek, J. Hradecky, V. Adam, O. Krystofova, D. Huska, M. Masarik, L. Trnkova, A. Horna, K. Klosova, M. Adamek, J. Zehnalek and R. Kizek, *Sensors*, 2007, **7**, 1238–1255.

[16] V. Vedharathinam and G. G. Botte, *Electrochim. Acta*, 2012, **81**, 292–300.

[17] S. Dubois, J. Colin, J. L. Duvail and L. Piraux, *Phys. Rev. B*, 2000, **61**, 14315–14318.

[18] L. Piraux, G. Hamoir, A. Encinas, J. de la Torre Medina and F. A. Araujo, *J. Appl. Phys.*, 2013, **114**, 123907.

[19] A. Ghaddar, J. Gieraltowski, F. Gloaguen, R. Zuberek, P. Aleshkevych, J. Kazmierczak, A. Slawska-Waniewska and H. Szymczak, *Acta Phys. Pol. A*, 2009, **116**, 1039–1043.

[20] C. T. Sousa, D. C. Leitao, M. P. Proenca, J. Ventura, A. M. Pereira and J. P. Araujo, *Appl. Phys. Rev.*, 2014, **1**, 031102.

[21] L. Sun, P. C. Searson and C. L. Chien, *Phys. Rev. B*, 2000, **61**, R6463–6466.

[22] X. W. Wang, G. T. Fei, X. J. Xu, Z. Jin and L. D. Zhang, *J. Phys. Chem. B*, 2005, **109**, 24326–24330.

[23] H. Pan, B. Liu, J. Yi, C. Poh, S. Lim, J. Ding, Y. Feng, C. H. A. Huan, and J. Lin, *J. Phys. Chem. B*, 2005, **109**, 3094–3098.

[24] K. Pitzschel, J. Bachmann, S. Martens, J. M. Montero-Moreno, J. Kimling, G. Meier, J. Escrig, K. Nielsch and D. Görlitz, *J. Appl. Phys.*, 2011, **109**, 033907.

[25] S. H. Xue and Z. D. Wang, *Mater. Sci. Eng., B*, 2006, **135**, 74–77.

[26] S. Karim and K. Maaz, *Mater. Chem. Phys.*, 2011, **130**, 1103 – 1108.

[27] B. Toal, M. McMillen, A. Murphy, W. Hendren, R. Atkinson and R. Pollard, *Mater. Res. Express*, 2014, **1**, 015801.

[28] M. Motoyama, Y. Fukunaka, T. Sakka and Y. H. Ogata, *J. Electrochem. Soc.*, 2006, **153**, C502–C508.

[29] I. Rahman, K. Razeeb, M. Rahman and M. Kamruzzaman, *J. Magn. Magn. Mater.*, 2003, **262**, 166–169.

[30] A. Cortés, G. Riveros, J. L. Palma, J. C. Denardin, R. E. Marotti, E. A. Dalchiele and H. Gómez, *J. Nanosci. Nanotechnol.*, 2009, **9**, 1992–2000.

[31] K. M. Razeeb, F. M. F. Rhen and S. Roy, *J. Appl. Phys.*, 2009, **105**, 083922.

[32] K. S. Napolskii, I. V. Roslyakov, A. A. Eliseev, D. I. Petukhov, A. V. Lukashin, S.-F. Chen, C.-P. Liu and G. A. Tsirlina, *Electrochim. Acta*, 2011, **56**, 2378 – 2384.

[33] S. Thongmee, H. Pang, J. Ding and J. Lin, *J. Magn. Magn. Mater.*, 2009, **321**, 2712 – 2716.

[34] F. Tian, Z. P. Huang and L. Whitmore, *Phys. Chem. Chem. Phys.*, 2012, **14**, 8537–8541.

[35] M. P. Proenca, C. T. Sousa, J. Ventura, M. Vazquez and J. P. Araujo, *Electrochim. Acta*, 2012, **72**, 215 – 221.

[36] J. de la Torre Medina, G. Hamoir, Y. Velázquez-Galván, S. Pouget, H. Okuno, L. Vila, A. Encinas and L. Piraux, *Nanotechnology*, 2016, **27**, 145702.

[37] Y. Yu, J. Li, J. Wang, X. Wu, C. Yu, T. Xu, B. Chang, H. Sun and H. Arandiyan, *Catalyst*, 2019, **9**, 152.

[38] S. Dellis, A. Christoulaki, N. Spiliopoulos, D. L. Anastassopoulos and A. A. Vradis, *J. Appl. Phys.*, 2013, **114**, 164308.

[39] H. S. Shin, J. Yu, J. Y. Song and H. M. Park, *Appl. Phys. Lett.*, 2009, **94**, 011906.

[40] H. S. Shin, J. Yu, J. Y. Song, H. M. Park and Y.-S. Kim, *Appl. Phys. Lett.*, 2010, **97**, 131903.

[41] X. W. Wang, G. T. Fei, L. Chen, X. J. Xu and L. D. Zhang, *Electrochem. Solid-State Lett.*, 2007, **10**, E1–E3.

[42] S.-Z. Chu, K. Wada, S. Inoue and S.-I. Todoroki, *Chem. Mater.*, 2002, **14**, 4595–4602.

[43] K. Nielsch, R. B. Wehrspohn, J. Barthel, J. Kirschner, S. F. Kronmüller, T. Schweinböck, D. Weiss and U. Gösele, *J. Magn. Magn. Mater.*, 2002, **249**, 234.

[44] C. A. Ross, M. Hwang, M. Shima, J. Y. Cheng, M. Farhoud, T. A. Savas, H. I. Smith, W. Schwarzacher, F. M. Ross, M. Redjdal and F. B. Humphrey, *Phys. Rev. B*, 2002, **65**, 144417.

[45] V. Vega, V. M. Prida, J. A. García and M. Vazquez, *Phys. Status Solidi A*, 2011, **208**, 553 – 558.

[46] J. Zhang, X. Qin, B. Torre, H. Zeng and X.-H. Xu, *IEEE Trans. Magn.*, 2014, **50**, 2301504.

[47] A. Encinas-Oropesa, M. Demand, L. Piraux, I. Huynen and U. Ebels, *Phys. Rev. B*, 2001, **63**, 104415.

[48] G. B. Harris, *Philos. Mag.*, 1952, **43**, 113 – 123.

[49] *ICDD PDA-4 Nickel, Card 00-004-0850*.

[50] E. Dalchiele, R. Marotti, A. Cortes, G. Riveros, H. Gómez, L. Martínez, R. Romero, D. Leinen, F. Martin and J. Ramos-Barrado, *Physica E*, 2007, **37**, 184–188.

[51] A. Encinas, M. Demand, J. M. George and L. Piraux, *IEEE Trans. Magn.*, 2002, **38**, 2574–2576.

[52] C. Kittel, *Introduction to Solid State Physics*, Wiley, New York, 6th edn., 1986.

[53] M. Tan and X. Chen, *J. Electrochem. Soc.*, 2011, **159**, K15–K20.

[54] X. H. Huang, G. H. Li, G. Z. Sun, X. C. Dou, L. Li and L. X. Zheng, *Nanoscale Res. Lett.*, 2010, **5**, 1057–1062.

[55] R. W. E Chassaing and, M Joussellin and, *J. Electroanal. Chem.*, 1983, **157**, 75–88.

[56] F. Maurer, G. T. Fei, X. J. Xu, Z. Jin and L. D. Zhang, *Nanotechnology*, 2007, **18**, 135709.

[57] J. Amblard, I. Epelboin, M. Froment and G. Maurin, *J. Appl. Electrochem.*, 1979, **9**, 233–242.

[58] M. Paunovic and M. Schlesinger, *Electrochemical Phase Formation and Growth*, Wiley-Interfase, New Jersey, 2006.

[59] K. Lejaeghere, V. V. Speybroeck, G. V. Oost and S. Cottenier, *Crit. Rev. Solid State Mater. Sci.*, 2014, **39**, 1.